THE JOURNAL OF PHYSICAL CHEMISTRY Letters

Letter

pubs.acs.org/JPCL

Vertically Aligned Carbon Nanotube Arrays Co-doped with Phosphorus and Nitrogen as Efficient Metal-Free Electrocatalysts for Oxygen Reduction

Dingshan Yu, Yuhua Xue, and Liming Dai*

Center of Advanced Science and Engineering for Carbon (Case4Carbon), Department of Macromolecular Science and Engineering, Case Western Reserve University, Cleveland, Ohio 44106, United States

Supporting Information

ABSTRACT: Using a mixture of ferrocene, pyridine, and triphenylphosphine as precursors for injection-assisted chemical vapor deposition (CVD), we prepared the first vertically aligned multiwalled carbon nanotube array co-doped with phosphorus (P) and nitrogen (N) with a relatively high P-doping level (designated as PN-ACNT). We have also demonstrated the potential applications of the resultant PN-ACNTs as high-performance electrocatalysts for the oxygen reduction reaction (ORR). PN-ACNT arrays were shown to exhibit a high ORR electrocatalytic activity, superb long-term durability, and good tolerance to methanol and carbon monoxide, significantly outperforming their counterparts doped with P (P-ACNT) or N (N-ACNT) only and even comparable to the commercially available Pt−C catalyst (45 wt % Pt on Vulcan XC-72R; E-TEK) due to a demonstrated synergetic effect arising from the co-doping of CNTs with both P and N.

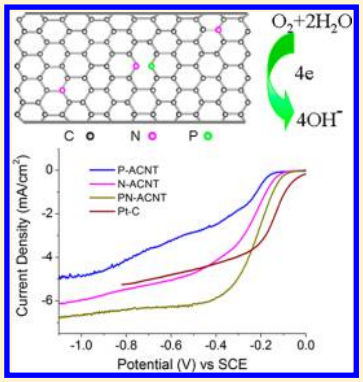

SECTION: Energy Conversion and Storage; Energy and Charge Transport

The fuel cell is one of the most promising clean and sustainable energy technologies that can directly convert chemical energy into electricity with a high efficiency by oxidizing fuel (e.g., H_2) at an anode and reducing oxygen gas at a cathode to produce water as the only waste. To make the fuel cell technology viable, catalysts are required to speed up the sluggish oxygen reduction reaction (ORR) at the cathode. During the past decades, considerable attention has been paid to the development of platinum and platinum-based alloy electrocatalysts for efficient ORR.[1−3] Although much progress has been achieved, the high cost and limited supply of platinum made the noble metal catalyst and its alloys unsuitable for large-scale production of fuel cells for commercial applications. Even though the amount of platinum needed for the desired catalytic effect could be reduced by using Pt alloys, commercial mass production would still require large amounts of platinum. Therefore, it is highly desirable to develop low-cost, efficient metal-free alternatives to replace Pt-based catalysts for ORR in fuel cells.[4−28]

Recent intensive research efforts in reducing/replacing the expensive platinum-based electrode for ORR have led to the development of nitrogen-doped carbon nanomaterials, including carbon nanotubes (CNTs), graphene, mesoporous graphitic arrays, mesoporous carbon, and carbon nitride, as metal-free ORR catalysts with superb electrocatalytic performance.[5,6,8−14,18,19] The improved catalytic performance was attributed to the net positive charge on carbon atoms in carbon nanomaterials created by the nitrogen dopants of a higher electronegativity than that of carbon.[5] The doping-induced charge redistribution changed the chemisorption mode of O_2 to effectively weaken the O−O bonding and also made the positively charged carbon atoms readily attract electrons from the anode to facilitate the ORR process.[5,6] Subsequently, the doping-induced ORR electrocatalytic effect was extended to include other doping atoms even with a lower electronegativity than that of carbon,[14] such as boron,[15] phosphorus,[16] and sulfur.[17] In these cases, it was found that the doping-induced charge redistribution, regardless of whether the dopants have a higher (as N) or lower (as B, P, S) electronegativity than that of carbon, could create charged sites (C^+, B^+, P^+, S^+) favorable for O_2 adsorption to facilitate the ORR process.[14] Furthermore, CNTs and graphene co-doped with more than one heteroatom, including boron and nitrogen co-doped CNTs[18] and graphene,[19] were developed to show even higher electrocatalytic activities for ORR than the corresponding single-atom doped counterparts due to a synergetic co-doping effect.[18] Recent studies have also shown that the incorporation of phosphorus into carbon−nitrogen nanostructures, including stacked carbon cup[27] and pyrolytic carbon from dicyandiamide,[28] enhanced the ORR activity in acidic electrolyte. As far as we are aware, however, the possibility of co-doping CNTs with N and P as metal-free ORR catalysts has not been exploited, though a few experimental and theoretical studies on the N and P co-doped CNTs for molecular detection have been

Received: August 14, 2012
Accepted: September 16, 2012
Published: September 17, 2012

reported recently.[29,30] Theoretical studies have predicted that defects induced by P doping or P−N co-doping can lead to the presence of a highly localized state close to the Fermi level, particularly attractive for electrochemical redox applications.[30−32] Although a previous report has demonstrated that P-doped graphitic layers could be used as metal-free catalysts for ORR, the reported electrocatalytic activity was much worse than that of the commercial Pt−C catalysts because of the low P-doping level (0.26 atom %).[16] It is still challenging to prepare P-doped CNT arrays with a high doping level because the P element cannot only reduce the activity of Fe catalysts required for the nanotube growth but also introduce disorders into the hexagonal carbon framework of the resultant nanotube due to its relatively larger atomic size with respect to the C atom.[21,22] Herein, we report the first successful synthesis of vertically aligned P−N co-doped multiwalled carbon nanotube arrays (i.e., PN-ACNTs) with a relatively high P content (P = 0.8 atom %, N = 2.9 atom %, C = 96.3 atom %) using a mixture of ferrocene, pyridine, and triphenylphosphine (TPP) as precursors by injection-assisted chemical vapor deposition (CVD). Owing to the previously demonstrated co-doping effect,[18] the resultant PN-ACNT arrays were demonstrated to exhibit a high ORR electrocatalytic activity, superb long-term stability, and good tolerance to methanol and carbon monoxide, significantly outperforming vertically aligned CNTs doped by P or N only and even comparable to the commercially available Pt−C catalyst (45 wt % Pt on Vulcan XC-72R; E-TEK).

In a typical experiment, a pyridine solution consisting of TPP (1 wt %) and ferrocene (2.5 wt %) was mechanically injected into a tube furnace at 760 °C under a H_2 flow of 150 sccm (sccm denotes cubic centimeter per minute at STP). After nanotube growth for 0.5 h, the furnace was cooled down to room temperature under an argon flow, instead of hydrogen, at the same flow rate. The resultant PN-ACNTs were then treated with HCl, followed by the reported electrochemical purification procedure,[5] to remove the residual iron nanoparticles.

Figure 1a and b reproduces typical side-view and top-view scanning electron microscope (SEM) images of the as-synthesized PN-ACNT arrays, showing well-aligned CNTs with almost no amorphous carbon. The tubular length is fairly uniform and approximately 15 μm for this particular PN-ACNT array grown for 0.5 h. Such relatively short nanotube arrays could facilitate the diffusion of electrolyte ions and oxygen molecules for the ORR process.[18] The energy dispersive X-ray spectroscopic (EDX) elemental mapping shown in Figure 1c−e indicates a uniform distribution for the nitrogen and phosphorus dopant atoms. The corresponding transmission electron microscope (TEM) image (Figure 1f) reveals that the purified individual P−N co-doped CNTs are indeed free from residual iron catalyst particles. These PN-ACNTs are about 20 nm in outer diameter and exhibit a typical bamboo-like structure.[33,34]

X-ray photoelectron spectroscopic (XPS) measurements were performed to gain more information about the chemical environments for the P and N atoms doped into the nanotube structure. As expected, the XPS survey spectrum given in Figure 2a shows the C 1s, N 1s, and P 2p peaks for the PN-ACNTs, along with an O 1s and associated Auger peaks. The O peaks arise, most probably, from the incorporation of physicochemically adsorbed oxygen, which was suggested to be advantageous for the ORR application.[18] The absence of any iron peak in the XPS survey spectrum confirms that the residual metal catalyst

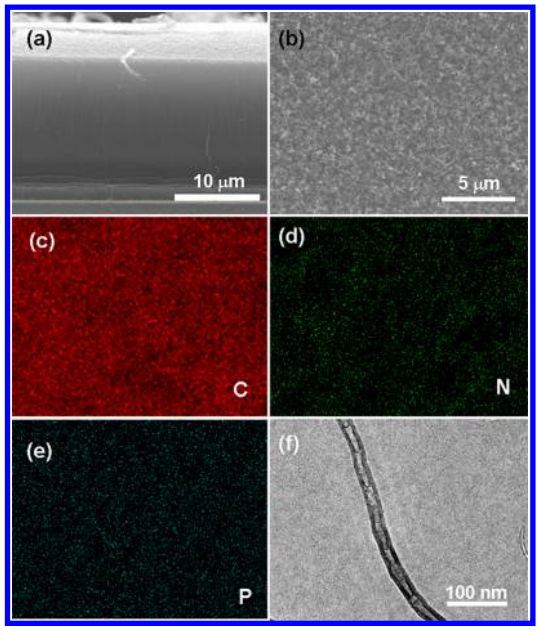

Figure 1. Typical cross-sectional (a) and top-view (b) SEM images, (c−e) EDX elemental mappings, and (f) a typical TEM image of an individual PN-ACNT.

particles, if any, have been completely removed by the mechanical transfer of the nanotube array from the growth substrate to the glassy carbon (GC) electrode and/or subsequent acid washing and electrochemical purification. The high-resolution C 1s peak at 284.7 eV shown in Figure 2b is very similar to that of graphite (HOPG),[35] and it can be deconvoluted into three different components. As can been from Figure 2b, the major component peak at about 284.7 eV indicates that graphite carbon is the majority.[36,37] A component peak that appeared at 285.9 eV is attributable to a C−N bond.[38] A very small broad band at 290−291 eV is attributed to a $\pi-\pi^*$ satellite, which is a common feature in XPS spectra of graphitic carbon.[37,38] These results indicate that the nanotube structure itself is almost free from C−O functionalities. The large O peak arises, as also demonstrated in the literature,[37,39] mainly from oxygen molecules absorbed on the carbon nanotube surface as carbon nanotubes are known to be susceptible to oxygen adsorption even at pressures as low as 10^{-8}−10^{-10} Torr.[37,39−41] As shown in Figure 2c, the N 1s peak at about 400 eV can be curve-fitted with two component peaks at 398.9 and 401.1 eV, corresponding to pyridinic- and graphitic-type N, respectively.[11] The P 2p peak at about 130 eV can be assigned mainly to the P−C bonding, which reveals that the P atom has been incorporated into the nanotube network.[16] The content of C (96.3 atom %) is dominant relative to P (0.8 atom %) and N (2.9 atom %). On the basis of our XPS results and the theoretical model proposed by Cruz-Silva et al.,[29] we drawn a schematic molecular structure for the PN-ACNT as a working hypothesis (Figure 2e).

To investigate the electrocatalytic activity of the PN-ACNT for ORR, we compared the electrocatalytic performance of the PN-ACNT arrays to those of the P-ACNT (1 atom % P), the N-ACNT (3.9 atom % N), and a commercial platinum−carbon catalyst (Pt−C, 45 wt % Pt on Vulcan XC-72R; E-TEK) by cyclic voltammetry (CV) in a nitrogen-protected or O_2-saturated aqueous solution of 0.1 M KOH. A constant active mass loading of the electrode materials (0.015 mg) was used for

dx.doi.org/10.1021/jz3011833 | J. Phys. Chem. Lett. 2012, 3, 2863−2870

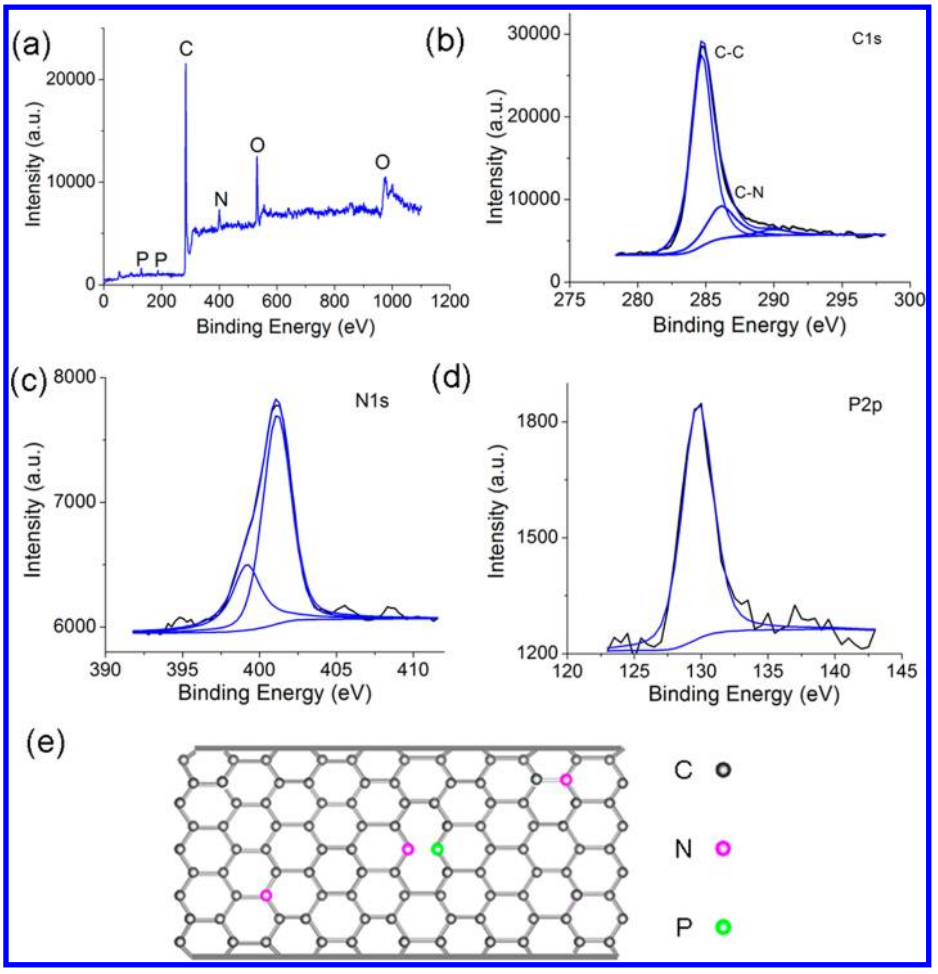

Figure 2. XPS spectra of PN-doped ACNTs: (a) survey spectrum; high-resolution (b) C 1s, (c) N 1s, and (d) P 2p; and (e) schematic representation of the possible P−N co-doped CNT structure.

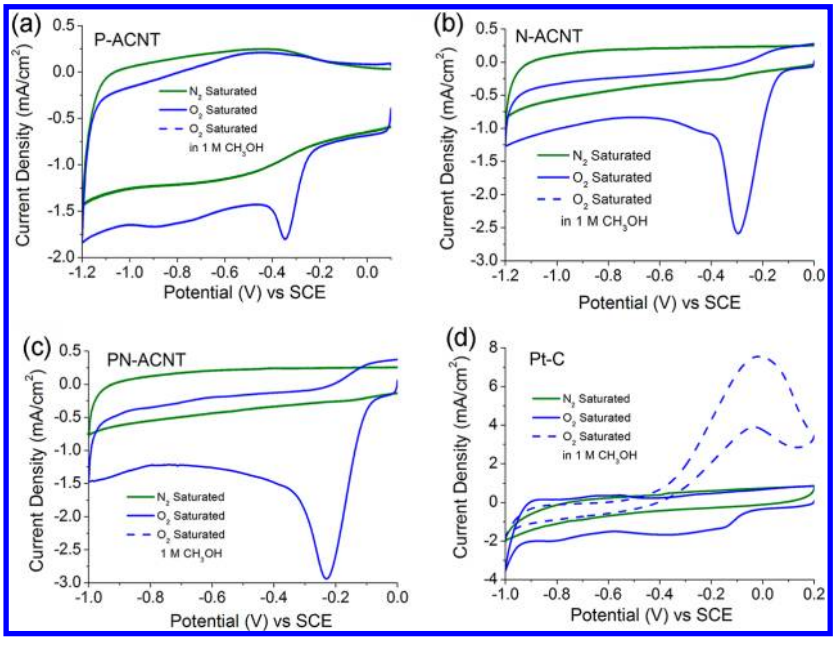

Figure 3. Typical cyclic voltammograms for the ORR at the (a) P-ACNT/GC electrode, (b) N-ACNT/GC electrode, (c) PN-ACNT/GC electrode, and (d) Pt−C/GC electrode in an aqueous solution of 0.10 M KOH saturated by nitrogen or oxygen gas or an oxygen-saturated 0.1 M solution of KOH upon addition of CH_3OH (1 M). Scan rate: 100 mV s^{-1}.

dx.doi.org/10.1021/jz3011833 | J. Phys. Chem. Lett. 2012, 3, 2863−2870

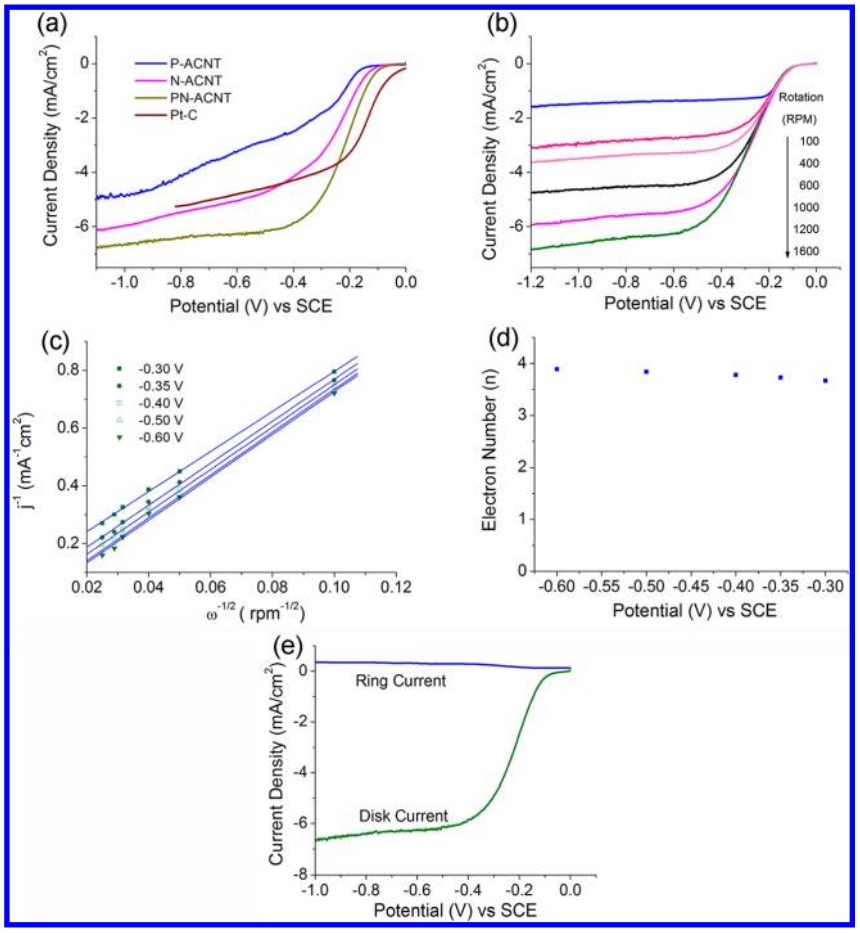

Figure 4. (a) RDE voltammograms of the P-ACNT/GC, N-ACNT/GC, PN-ACNT/GC, and Pt−C/GC electrodes in an oxygen-saturated, 0.10 M KOH solution at a rotation rate of 1600 rpm. Scan rate: 10 mV s^{-1}. (b) RDE voltammograms of the PN-ACNT/GC electrode in an O_2-saturated, 0.1 M KOH solution at a scan rate of 10 mV s^{-1} and at different rotation rates. (c) Koutecky−Levich plot of j^{-1} versus $\omega^{-1/2}$ at different electrode potentials of −0.30, −0.35, −0.40, −0.50, and −0.60 V. (d) The dependence of transferred electron number (n) on the potential. The experimental data were obtained from (c). (e) RRDE voltammograms of the PN-ACNT/GC electrode in an O_2-saturated, 0.1 M KOH aqueous solution at a scan rate of 10 mV s^{-1} at 1600 rpm.

all of the electrodes. As can be seen in Figure 3, all three CNT-based electrodes showed substantial reduction current in the presence of oxygen, whereas no noticeable response was observed under nitrogen. Comparison of the onset and peak potentials between the P-ACNT and N-ACNT electrodes shows that N doping is more efficient than P doping toward ORR; athough, because of its relatively low nitrogen content, the A-NCNT (3.9 at% N) produced by pyrolysis of ferrocene in the presence of ammonia (see the Supporting Information) used in this study did not exhibit the record high ORR activity reported for its counterpart from pyrolysis of iron(II) phthalocyanine (5.6 atom % N).[5] In terms of the onset and peak potentials as well as the current density, the PN-ACNT electrode is most active among all of the CNT-based electrodes used in this study due to a synergetic effect that resulted from co-doping of the CNTs with N and P, as is the case with the N and B co-doped carbon nanomaterials.[18,19] Given the same loading mass (0.015 mg) of active materials that was used, the PN-ACNT electrode even outperformed the commercial Pt−C electrode in terms of the current density as the maximum oxygen reduction current density of the PN-ACNT/GC electrode at about −0.22 V (Figure 3c) was much higher than that of the Pt−C/GC electrode at about −0.13 V (Figure 3d) in the same oxygen-saturated alkaline solution.

To examine the possible crossover effect, we measured the electrocatalytic selectivity of P-ACNT, N-ACNT, PN-ACNT, and Pt−C/GC electrodes, respectively, against the electro-oxidation of methanol by CV in an O_2-saturated aqueous solution of 0.1 M KOH after the addition of 1 M methanol. Upon the methanol addition, the cathodic signals for the ORR at about −0.13 V disappeared in CV curves for the Pt−C/GC electrode (Figure 3d). In the meantime, the current intensity corresponding to methanol oxidation at the Pt−C/GC electrode reached up to ∼7.5 mA cm^2 at −0.03 V (Figure 3d). However, no noticeable change was observed for the P-ACNT, N-ACNT, and PN-ACNT/GC electrodes under the same conditions (Figure 3a−c; the dashed blue curves overlapped with the solid blue curves), as is the case for N-doped mesoporous graphitic arrays[11] and P-doped graphite.[16] These results indicate that all of the CNT catalysts possess much higher selectivity for the ORR with almost no methanol crossover effect than the Pt−C catalyst, as previously demonstrated for other carbon-based ORR electrodes.[5−15]

We further compared the electrocatalytic activity of the PN-ACNT electrode with that of the P-ACNT, N-ACNT, and commercial Pt−C catalysts by linear sweep voltammetry in an aqueous solution of O_2-saturated, 0.1 M KOH at a rotation rate of 1600 rpm and a scan rate of 10 mV s^{-1}. For all of the

dx.doi.org/10.1021/jz3011833 | J. Phys. Chem. Lett. 2012, 3, 2863−2870

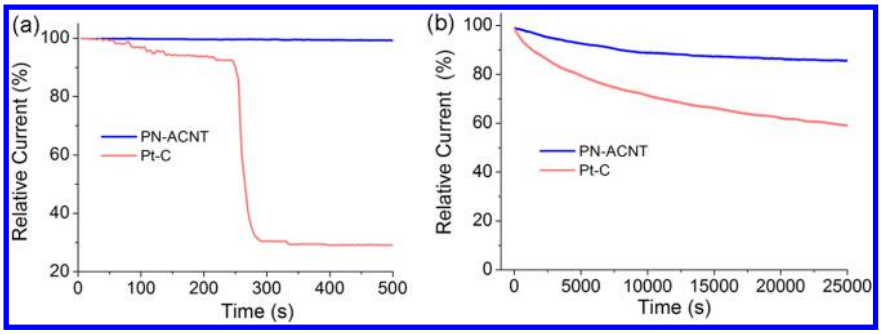

Figure 5. (a) Current−time (j−t) chronoamperometric response for ORR at the PN-ACNT/GC electrode and the Pt−C/GC electrode upon introduction of CO after about 250 s at −0.25 V. (b) Chronoamperometric response of the PN-ACNT/GC electrode and the Pt−C/GC electrode at −0.25 V in an O_2-saturated 0.10 M KOH aqueous solution.

electrodes, the LSV curves show a single-step wide platform, indicating a four-electron ORR process.[5,18] The onset potential of the PN-ACNT/GC electrode for the ORR is at approximately −0.09 V, which is more positive than those of the P-ACNT/GC electrode (−0.17 V) and the N-ACNT/GC (−0.13 V). Furthermore, the diffusion-limited current density from the PN-ACNT/GC electrode is also much higher than those of the P-ACNT/GC and N-ACNT/GC electrodes. Once again, the PN-ACNT electrode showed the best electrocatalytic activity toward ORR among all nanotube electrodes studied in the present work. Although the onset potential for the PN-ACNT/GC electrode was still a little bit more negative than that of the Pt−C/GC electrode (∼−0.01 V), the PN-ACNT/GC electrode showed a much stronger oxygen-reduction current density with respect to the Pt−C/GC (Figures 3 and 4a).

To gain more information on kinetics of the PN-ACNT catalyst during the ORR process, we performed the rotating disk electrode (RDE) measurements in an O_2-saturated, 0.1 M KOH aqueous solution at a scan rate of 10 mV s^{-1} and different rotation rates (Figure 4b). As seen in Figure 4b, the RDE voltammetric profiles showed that the diffusion current density increased with an increase in the rotation rate (from 100 to 1600 rpm). The transferred electron number (n) per oxygen molecule involved in the ORR process was further determined by the Koutecky−Levich equation, which relates the current density j to the rotation rate of the electrode ω by eq 1.[42]

$$\frac{1}{j} = \frac{1}{j_k} + \frac{1}{B\omega^{0.5}} \tag{1}$$

where j_k is the kinetic current density and B is related to the diffusion-limiting current density expressed by the following expression[18,42]

$$B = 0.2nF(D_{O_2})^{2/3}\nu^{-1/6}C_{O_2} \tag{2}$$

where n is the overall number of electrons transferred during the oxygen reduction, F is the Faraday constant (F = 96485 C mol^{-1}), C_{O_2} is the bulk concentration of O_2 (1.2×10^{-6} mol cm^{-3}), D_{O_2} is the diffusion coefficient of O_2 in the KOH electrolyte (1.9×10^{-5} cm^2 s^{-1}), and ν is the kinetic viscosity of the electrolyte (0.01 cm^2 s^{-1}). The constant 0.2 is adopted when the rotation speed is expressed in rpm. The corresponding Koutecky−Levich plots (j^{-1} versus $\omega^{-1/2}$) at various electrode potentials exhibited a good linearity with an almost constant slope over the potential range from −0.3 to −0.6 V (Figure 4c), suggesting first-order reaction kinetics for ORR. The electron transfer numbers (n) were calculated from the slopes of Koutecky−Levich plots to be 3.67−3.88 at the potential ranging from −0.3 to 0.6 V, indicating a four-electron process toward ORR on the PN-ACNT electrode. This is further confirmed by the negligible ring current recorded at a rotating ring disk electrode (RRDE, Figure 4e). The corresponding electron-transfer numbers per oxygen molecule for ORR at the P-ACNT and the N-ACNT electrodes are 3.02 and 3.75, respectively, at the potential of −0.4 V according to the RRDE measurements.

To investigate the CO poisoning effect and the electrochemical stability of the PN-ACNT electrode, we introduced 12 vol % CO/O_2 into the electrolyte solution (i.e., an O_2-saturated 0.10 M KOH aqueous solution) during the j−t chronoamperometric measurements at the PN-ACNT/GC electrode with the Pt−C/GC electrode as a reference. As seen in Figure 5a, the PN-ACNT electrode was insensitive to the CO addition, while the Pt/C electrode was rapidly poisoned under the identical conditions.

Finally, the PN-ACNT electrode was subjected to a chronoamperometric durability test at a constant voltage of −0.25 V for 25000 s in an aqueous solution of 0.1 M KOH saturated with O_2 at a rotation rate of 1600 rpm. Figure 5b shows that the j−t chronoamperometric response of the PN-ACNT/GC electrode exhibited a very slow attenuation with a high current retention (85%) even after 25000 s. In contrast, the corresponding j−t response for the Pt−C/GC electrode exhibited a gradual decrease with a current loss of approximately 43% after 25000 s. These results suggest that the PN-ACNT electrode has a much better stability than the Pt−C catalyst. The Pt and other metal catalysts are known to gradually degrade over time due to surface oxidation and particle dissolution/aggregation, particularly in the alkaline electrolytes used for alkaline fuel cells.[43,44] Because it has been one of the major challenges to improve the catalyst durability for alkaline fuel cells, the PN-ACNT electrode with the demonstrated superb ORR electrocatalytic activity and excellent stability is particularly attractive for ORR in alkaline solutions for fuel cells and many other electrocatalytic reduction systems (e.g., lithium−air batteries, DSSCs, electrochemical biosensors).

In summary, we have demonstrated the first synthesis of vertically aligned MWCNT arrays co-doped with P and N using a mixture of ferrocene, pyridine, and TPP as precursors by an injection-assisted CVD method. Owing to a synergetic effect arising from co-doping CNTs with both P and N, the resultant P−N co-doped carbon nanotubes were demonstrated to show a significantly enhanced electrocatalytic activity toward ORR with

dx.doi.org/10.1021/jz3011833 | J. Phys. Chem. Lett. 2012, 3, 2863−2870

respect to CNTs doped by P or N only, even comparable to the commercial Pt−C electrode. The superior ORR activity, together with the excellent long-term stability and good tolerance to methanol crossover and CO poisoning effects as well as the relatively simple nanotube growth process, makes the vertically aligned P−N co-doped CNT arrays ideal low-cost and highly efficient metal-free ORR catalysts for alkaline fuel cells and many other electrocatalytic reduction systems, including lithium−air batteries, DSSCs, and electrochemical biosensors.

EXPERIMENTAL METHODS

Synthesis of Phosphorus−Nitrogen Co-doped Vertically Aligned Carbon Nanotubes (PN-ACNTs). PN-ACNTs were synthesized using a mixture of ferrocene, pyridine, and triphenylphosphine (TPP) as precursors by injection-assisted chemical vapor deposition (CVD). SiO_2/Si substrate sputter-coated with Ni/Fe (5 nm/5 nm) was used as the substrate for the nanotube growth. Briefly, a solution with 1 wt % of TPP and 2.5 wt % of ferrocene dissolved in pyridine was pyrolyzed inside of a tube furnace operated at 760 °C with a H_2 flow of 150 sccm (sccm denotes cubic centimeter per minute at STP). After the CNT growth for 0.5 h, the furnace was cooled down to room temperature under an argon flow, instead of hydrogen, at the same flow rate. The resultant PN-ACNTs were treated with HCl and subjected to electrochemical purification according to a reported procedure[5] to remove the residual iron nanoparticles used for the nanotube growth. The P and N contents were determined to be about 0.8 and 2.9 atom % by XPS measurements.

Synthesis of Phosphorus-Doped Vertically Aligned Carbon Nanotubes (P-ACNTs). P-ACNTs were prepared by the CVD method using toluene and ferrocene as the carbon and catalyst sources and TPP as the P precursor. Commercially available SiO_2/Si wafers sputter-coated with Ni/Fe (5 nm/5 nm) were used as the substrate for the P-ACNT growth. In a typical process, a toluene solution (3 mL) containing 2 wt % TPP and 2.5 wt % ferrocene was injected, along with a H_2 flow (150 sccm), over the SiO_2/Si substrate at 760 °C in a quartz tube furnace. After the nanotube growth for 0.5 h, P-ACNTs supported by the SiO_2/Si substrate were removed quickly from the reaction zone and cooled down to room temperature under an Ar flow (150 sccm). The P content in the P-doped ACNT was determined to be about 1 atom % by XPS measurements (to see Figure S2, Supporting Information).

Synthesis of N-Doped Vertically Aligned Carbon Nanotubes (N-ACNTs). N-ACNTs used in this study were prepared by pyrolysis of ferrocene in the presence of ammonia. In a typical experiment, 3 mL of 2 wt % ferrocene in toluene solution was injected, along with a mixture gas flow of NH_3 (30 sccm)/H_2 (60 sccm)/Ar (60 sccm), over the SiO_2/Si substrate at 780 °C for 10 min. Upon completion of the nanotube growth, the resultant N-ACNTs supported by the SiO_2/Si substrate were removed quickly from the reaction zone and cooled down to room temperature under an Ar/H_2 flow. The N content in the N-doped ACNT was determined to be about 3.9 atom % by XPS measurements (to see Figure S2, Supporting Information).

The N content of N-ACNT grown from ferrocene/NH_3 at 780 °C is 3.9 atom % (pyridinic 27.2%; graphitic 72.8%). The ORR activity on the N-ACNTs grown from ferrocene/NH_3 in the present study seems not as good as our previously reported result in ref 5 for the N-ACNTs produced from iron phthalocyanine (FePc)/NH_3. This is because the FePc-generated A-NCNTs possesses a relatively high N content of 5.6 atom % (pyridinic 70%; pyrrole-like 30%; see Table S1 and Figure S2 in the Supporting Information of ref 5), along with a much higher content of pyridinic nitrogen (70%) with respect to that of VA-NCNT produced from ferrocene/NH_3 (27.2%). Pyridinic nitrogen has been demonstrated to be most ORR-active among all of the nitrogen species.[6] The ferrocene-generated VA-NCNTs are used in this study to be consistent with other nanotubes synthesized in this work; for example, TPP/ferrocene were used for the growth of P-doped ACNTs.

Materials Characterization. The morphology and structure of the nanotube arrays were analyzed by scanning electron microscopy (SEM, Hitachi S4800-F) and transmission electron microscopy (TEM, JEOL JEM-2100). XPS measurements were performed on a VG Microtech ESCA 2000 using a monochromic Al X-ray source (97.9 W, 93.9 eV).

Electrochemical Measurements. Electrochemical measurements were performed on a computer-controlled potentiostat (CHI 760C, CH Instrument, U.S.A.) with a three-electrode electrochemical cell. A platinum wire was used as the counter electrode, and a saturated calomel electrode (SCE) was used as the reference electrode. All of the experiments were conducted at room temperature (25 ± 1 °C). The P−N co-doped ACNT and other nanotube arrays were transferred onto the glassy carbon electrode (GCE, 5 mm diameter) according to the following procedure: PN-ACNTs on the SiO_2/Si substrate were first immersed in HF aqueous solution (1 wt % HF) for 5 min to peel the PN-ACNT from the SiO_2/Si substrate,[34,45] which were then transferred onto the GC electrode, followed by casting with a Nafion solution (0.05 wt % in isoproponal) as the bonder. Prior to electrochemical measurements, all of the carbon-based electrode materials, including the PN-ACNT, P-ACNT, and N-ACNT nanotubes, were subjected to the electrochemical purification to completely remove the metal catalyst residues, if any, according to the published procedure.[5] The activity of the electrocatalysts was evaluated by CV and linear sweep voltammetry techniques on rotating disk electrodes (RDEs) and rotating ring disk electrodes (RRDEs). Durability testing for the PN-ACNT nanotube electrode and the Pt/C electrocatalyst was conducted by the chronoamperometric technique at −0.25 V (versus SCE) in an oxygen-saturated aqueous solution of 0.1 M KOH up to 25 000 s.

ASSOCIATED CONTENT

Supporting Information

SEM and XPS images of N- and P-doped ACNT. This material is available free of charge via the Internet at http://pubs.acs.org.

AUTHOR INFORMATION

Corresponding Author

*E-mail: Liming.Dai@case.edu.

Notes

The authors declare no competing financial interest.

ACKNOWLEDGMENTS

We thank the support from AFOSR (FA-9550-12-1-0069, FA 9550-10-1-0546, FA9550-12-1-0037), NSF-CMMI-1047655, NSFC-NSF MWN (NSF-DMR 1106160), DOD-Army (W911NF-11-1-0209), and DAGSI (RX2-CWRU-10-1).

REFERENCES

(1) Stamenkovic, V. R.; Fowler, B.; Mun, B. S.; Wang, G. J.; Ross, P. N.; Lucas, C. A.; Markovic, N. M. Improve Oxygen Reduction Activity on $Pt_3Ni(111)$ via Increased Surface Site Availability. *Science* **2007**, *315*, 493−497.

(2) Peng, Z.; Yang, H. Synthesis and Oxygen Reduction Electrocatalytic Property of Pt-on-Pd Bimetallic Heteronanostructures. *J. Am. Chem. Soc.* **2009**, *131*, 7542−7543.

(3) Xiao, L.; Zhuang, L.; Liu, Y.; Lu, J. T.; Abruna, H. D. Activating Pd by Morphology Tailoring for Oxygen Reduction. *J. Am. Chem. Soc.* **2009**, *131*, 602−608.

(4) Wang, X.; Lee, J. S.; Zhu, Q.; Liu, J.; Wang, Y.; Dai, S. Ammonia-Treated Ordered Mesoporous Carbons As Catalytic Materials for Oxygen Reduction Reaction. *Chem. Mater.* **2010**, *22*, 2178−2180.

(5) Gong, K. P.; Du, F.; Xia, Z. H.; Durstock, M.; Dai, L. M. Nitrogen-Doped Carbon Nanotube Arrays with High Electrocatalytic Activity for Oxygen Reduction. *Science* **2009**, *323*, 760−764.

(6) Yu, D.; Nagelli, E.; Du, F.; Dai, L. Metal-Free Carbon Nanomaterials Become More Active than Metal Catalysts and Last Longer. *J. Phys. Chem. Lett.* **2010**, *1*, 2165−2173.

(7) Wang, S.; Yu, D.; Dai, L. Polyelectrolyte Functionalized Carbon Nanotubes as Efficient Metal-Free Electrocatalysts for Oxygen Reduction. *J. Am. Chem. Soc.* **2011**, *133*, 5182−5184.

(8) Qu, L. T.; Liu, Y.; Baek, J. B.; Dai, L. M. Nitrogen-Doped Graphene as Efficient Metal-Free Electrocatalyst for Oxygen Reduction in Fuel Cells. *ACS Nano* **2010**, *4*, 1321−1326.

(9) Yu, D.; Zhang, Q.; Dai, L. Highly Efficient Metal-Free Growth of Nitrogen-Doped Single-Walled Carbon Nanotubes on Plasma-Etched Substrates for Oxygen Reduction. *J. Am. Chem. Soc.* **2010**, *132*, 15127−15129.

(10) Sun, Y.; Li, C.; Shi, G. Nanoporous Nitrogen Doped Carbon Modified Graphene as Electrocatalyst for Oxygen Reduction Reaction. *J. Mater. Chem.* **2012**, *22*, 12810−12816.

(11) Liu, R. L.; Wu, D. Q.; Feng, X. L.; Mullen, K. Nitrogen-Doped Ordered Mesoporous Graphitic Arrays with High Electrocatalytic Activity for Oxygen Reduction. *Angew. Chem., Int. Ed.* **2010**, *49*, 2565−2569.

(12) Yang, W.; Fellinger, T; Antonietti, M. Efficient Metal-Free Oxygen Reduction in Alkaline Medium on High-Surface-Area Mesoporous Nitrogen-Doped Carbons Made from Ionic Liquids and Nucleobases. *J. Am. Chem. Soc.* **2011**, *133*, 206−208.

(13) Liang, J.; Zheng, Y.; Chen, J.; Liu, J.; Hulicova-Jurcakova, D.; Jaroniec, M.; Qiao, S. Z. Facile Oxygen Reduction on a Three-Dimensionally Ordered Macroporous Graphitic C3N4/Carbon Composite Electrocatalyst. *Angew. Chem., Int. Ed.* **2012**, *124*, 3958−3962.

(14) Zhang, M.; Dai, L. Carbon Nanomaterials as Metal-Free Catalysts in Next Generation Fuel Cells. *Nano Energy* **2012**, *4*, 514−517.

(15) Yang, L.; Jiang, S.; Zhao, Y.; Zhu, L.; Chen, S; Wang, X.; Wu, Q.; Ma, J.; Ma, Y.; Hu., Z. Boron-Doped Carbon Nanotubes as Metal-Free Electrocatalysts for the Oxygen Reduction Reaction. *Angew. Chem., Int. Ed.* **2011**, *50*, 7132−7135.

(16) Liu, Z. W.; Peng, F.; Wang, H.-J.; Yu, H.; Zheng, W.-X.; Yang, J. Phosphorus-Doped Graphite Layers with High Electrocatalytic Activity for the O_2 Reduction in an Alkaline Medium. *Angew. Chem., Int. Ed.* **2011**, *50*, 3257−3261.

(17) Yang, Z.; Yao, Z.; Li, G.; Fang, G.; Nie, H.; Liu, Z.; Zhou, X.; Chen, X.; Huang, S. Sulfur-Doped Graphene as an Efficient Metal-Free Cathode Catalyst for Oxygen Reduction. *ACS Nano* **2012**, *6*, 205−211.

(18) Wang, S.; Iyyamperumal, E.; Roy, Ajit.; Xue, Y.; Yu, D. S.; Dai, L. Vertically Aligned BCN Nanotubes as Efficient Metal-Free Electrocatalysts for the Oxygen Reduction Reaction: A Synergetic Effect by Co-Doping with Boron and Nitrogen. *Angew. Chem., Int. Ed.* **2011**, *50*, 11756−11670.

(19) Wang, S.; Zhang, L.; Xia, Z.; Roy, A.; Chang, D.; Baek, J. B.; Dai, L. BCN Graphene as Efficient Metal-Free Electrocatalyst for the Oxygen Reduction Reaction. *Angew. Chem., Int. Ed.* **2012**, *51*, 4209−4212.

(20) Chen, Z. W.; Higgins, D. C.; Yu, A.; Zhang, L.; Zhang, J. A Review on Non-precious Metal Electrocatalysts for PEM Fuel Cells. *Energy Environ. Sci.* **2011**, *4*, 3167−3192.

(21) Rao, C. V.; Ishikawa, Y. Activity, Selectivity, and Anion-Exchange Membrane Fuel Cell Performance of Virtually Metal-Free Nitrogen-Doped Carbon Nanotube Electrodes for Oxygen Reduction Reaction. *J. Phys. Chem. C* **2012**, *116*, 4340−4346.

(22) Wiggins-Camacho, J. D.; Stevenson, K. J. Mechanistic Discussion of the Oxygen Reduction Reaction at Nitrogen-Doped Carbon Nanotubes. *J. Phys. Chem. C* **2011**, *115*, 20002−20010.

(23) Wiggins-Camacho, J. D.; Stevenson, K. J. Effect of Nitrogen Concentration on Capacitance, Density of States, Electronic Conductivity, and Morphology of N-Doped Carbon Nanotube Electrodes. *J. Phys. Chem. C* **2009**, *113*, 19082−19090.

(24) Yang, S. B.; Feng, X. L.; Wang, X.; Mullen, K. Graphene-Based Carbon Nitride Nanosheets as Efficient Metal-Free Electrocatalysts for Oxygen Reduction Reactions. *Angew. Chem., Int. Ed.* **2011**, *50*, 5339−5343.

(25) Rao, C. V.; Cabrera, C. R.; Ishikawa, Y. In Search of the Active Site in Nitrogen-Doped Carbon Nanotube Electrodes for the Oxygen Reduction Reaction. *J. Phys. Chem. Lett.* **2010**, *1*, 2622−2627.

(26) Kim, H.; Lee, K.; Woo, S.; Jung, Y. On the Mechanism of Enhanced Oxygen Reduction Reaction in Nitrogen-Doped Graphene Nanoribbons. *Phys. Chem. Chem. Phys.* **2011**, *13*, 17505−17510.

(27) Deak, D.; Biddinger, E. J.; Luthman, K.; Ozkan, U. S. The Effect of Phosphorus in Nitrogen-Containing Carbon Nanostructures on Oxygen Reduction in PEM Fuel Cells. *Carbon* **2010**, *48*, 3635−3658.

(28) Choi, C. H.; Park, S. H.; Woo, S. Binary and Ternary Doping of Nitrogen, Boron, and Phosphorus into Carbon for Enhancing Electrochemical Oxygen Reduction Activity. *ACS Nano* **2012**, *6*, 7084−7091.

(29) Cruz-Silva, E.; Lopez-Urias, F.; Munoz-Sandoval, E.; Sumpter, B. G.; Terrones, H.; Charlier, J. C.; Meunier, V.; Terrones, M. Phosphorus and Phosphorus−nitrogen Doped Carbon Nanotubes for Ultrasensitive and Selective Molecular Detection. *Nanoscale* **2011**, *3*, 1008−1013.

(30) Cruz-Silva, E.; Cullen, D. A.; Gu, L.; Romo-Herrera, J. M.; Muñoz-Sandoval, E.; López-Urías, F.; Sumpter, B. G.; Meunier, V.; Charlier, J. C.; Smith, D. J.; et al. Heterodoped Nanotubes: Theory, Synthesis, and Characterization of Phosphorus-Nitrogen Doped Multiwalled Carbon Nanotubes. *ACS Nano* **2008**, *2*, 441−448.

(31) Maciel, I. O.; Campos-Delgado, J.; Cruz-Silva, E.; Pimenta, M. A.; Sumpter, B. G.; Meunier, V.; Lopez-Urias, F.; Munoz-Sandoval, E.; Terrones, H.; Terrones, M.; Jorio, A. Synthesis, Electronic Structure, and Raman Scattering of Phosphorus-Doped Single-Wall Carbon Nanotubes. *Nano Lett.* **2009**, *9*, 2267−2272.

(32) Strelko, V. V.; Kuts, V. S.; Thrower, P. A. On the Mechanism of Possible Influence of Heteroatoms of Nitrogen, Boron, and Phosphorus in a Carbon Matrix on the Catalytic Activity of Carbons in Electron Transfer Reactions. *Carbon* **2000**, *38*, 1499−525.

(33) Li, D. C.; Dai, L.; Huang, S.; Mau, A. W. H.; Wang, Z. L. Structure and Growth of Aligned Carbon Nanotube Films by Pyrolysis. *Chem. Phys. Lett.* **2000**, *316*, 349−355.

(34) Dai, L. Advanced Syntheses and Microfabrications of Conjugated Polymers, C60-Containing Polymers, and Carbon Nanotubes for Optoelectronic Applications. *Polym. Adv. Technol.* **1999**, *10*, 357−420.

(35) Chen, Q.; Dai, L.; Gao, M.; Huang, S.; Mau, A. W. H. Plasma Activation of Carbon Nanotubes for Chemical Modification. *J. Phys. Chem. B* **2001**, *105*, 618−622 and references cited therein.

(36) Pels, J. R.; Kapteijn, F.; Moulijn, J. A.; Zhu, Q.; Thomas, K. M. Evolution of Nitrogen Functionalities in Carbonaceous Materials during Pyrolysis. *Carbon* **1995**, *33*, 1641−1653.

(37) Shalagina, A. E.; Ismagilov, Z. R.; Podyacheva, O. Y.; Kvon, R. I.; Ushakov, V. A. Synthesis of Nitrogen-Containing Carbon Nanofibers by Catalytic Decomposition of Ethylene/Ammonia Mixture. *Carbon* **2007**, *45*, 1808−1820.

(38) Maldonado, S.; Morin, S.; Stevenson, K. J. Structure, Composition, and Chemical Reactivity of Carbon Nanotubes by Selective Nitrogen Doping. *Carbon* **2006**, *44*, 1429−1437.
(39) Collins, P. G.; Bradley, K.; Ishigami, M.; Zettl, A. Extreme Oxygen Sensitivity of Electronic Properties of Carbon Nanotubes. *Science* **2000**, *287*, 1801−1804.
(40) He, M.; Zhou, S.; Zhang, J.; Liu, Z.; Robinson, C. CVD growth of N-Doped Carbon Nanotubes on Silicon Substrates and its Mechanism. *J. Phys. Chem. B* **2005**, *109*, 9275−9279.
(41) Liu, H.; Zhang, Y.; Li, R. Y.; Sun, X. L.; Desilets, S.; Abou-Rachid, H.; Jaidann, M.; Lussier, L. Structural and Morphological Control of Aligned Nitrogen Doped Carbon Nanotubes. *Carbon* **2010**, *48*, 1498−1507.
(42) Paulus, U. A.; Wokaun, A.; Scherer, G. G.; Schmidt, T. J.; Stamenkovic, V.; Radmilovic, V.; Markovic, N. M.; Ross, P. N. Oxygen Reduction on Carbon-Supported Pt−Ni and Pt−Co Alloy Catalysts. *J. Phys. Chem. B* **2002**, *106*, 4181−4191.
(43) Gewirth, A. A.; Thorum, M. S. Electroreduction of Dioxygen for Fuel-Cell Applications: Materials and Challenges. *Inorg. Chem.* **2010**, *49*, 3557−3566.
(44) Spendelow, J. S.; Wieckowski, A. Electrocatalysis of Oxygen Reduction and Small Alcohol Oxidation in Alkaline Media. *Phys. Chem. Chem. Phys.* **2007**, *9*, 2654−2675.
(45) Chen, Q.; Dai, L. Plasma Patterning of Carbon Nanotubes. *Appl. Phys. Lett.* **2000**, *76*, 2719 and references cited therein.